Suppressing vibration errors in phase-shifting interferometry

Leslie L. Deck

Zygo Corporation, Laurel Brook Road, Middlefield, CT. USA, 06455-0448

ABSTRACT

A new method for reducing the influence of vibrations in phase-shifting interferometry uses spatial information to achieve a 100X reduction in vibrationally induced surface distortion for small-amplitude vibrations. The technique does not require high density spatial carrier fringes and maintains full lateral sampling resolution. The principles of the technique are discussed and calculations highlight the capabilities, supported by real measurements under a variety of vibration conditions.

1. INTRODUCTION

Interferometric surface profilers incorporating phase-shifting interferometry (PSI) techniques[1] now routinely measure surfaces with nanometer level vertical resolution, but still suffer from sensitivity to environmental vibrations. Passive isolation components such as air tables are common auxiliaries in interferometric metrology systems and for the most part work well enough for interferometers to have become ubiquitous tools for precision measurements, but the sensitivity of these systems to vibration is often the barrier to further improvement.

The vibration sensitivity of PSI methods rests fundamentally on the measurement principle. Phase-shifting techniques analyze the intensity variation from a controlled phase shift to determine the starting phase of the interferogram. Vibration produces unknown, time dependent changes to the phase shift, which the analysis then falsely interprets as a surface variation. The manifestation of this error is a periodic deformation of the measured surface, often called ripple, with a spatial frequency equal to twice the fringe frequency. This 2-cycle deformation, which can be readily understood in terms of a Fourier description of the technique,[2] occurs for all vibration frequencies.

Previous PSI vibration error suppression techniques can be broadly divided into three basic categories. The simplest is to acquire PSI data at higher rates to freeze vibrations and to enable intensive averaging.[3, 4, 5] An alternative approach is to remove the time element entirely by acquiring the phase shifted intensity information simultaneously. These techniques[6, 7, 8] derive the interferometric phase at the same instant in time, but usually at the expense of a system attribute, such optical common path, lateral resolution, polarization insensitivity or cost. The third category minimizes errors by attempting to measure the true phase shift increment between intensity samples.[9, 10, 11, 12] The appeal here is that the interferometer geometry or apparatus need not change and there is little compromise in measurement precision relative to traditional PSI.

I discuss a new post-processing technique in this paper, called Vibration Compensated PSI (VC)[13], which has attributes common to the last two categories. It overcomes many of the difficulties of previous methods; it is swiftly and easily calculated, it can be applied to any PSI acquisition, there are few restrictions on surface shape and only one fringe is required in the image. The goal of the technique is not to achieve vibration immunity, but rather to improve PSI instruments and techniques to reach a higher level of performance in the presence of vibrations found in standard practice.

2. VIBRATION SENSITIVITY IN PSI

To provide a mathematical description of vibrationally induced phase errors in phase-shifting interferometry, I start by writing the interference intensity variation during a PSI acquisition in the presence of a pure vibrational tone as:

$$I(\mathbf{x},t) = I_0\left\{1 + V\cos\left[\Phi(\mathbf{x}) + 2\pi\nu_0 t + r\cos(2\pi\nu_v t + \alpha)\right]\right\} \quad (1)$$

where I_0 is the average intensity, V the contrast, ν_0 is the fundamental interference frequency of the PSI acquisition, ν_v is the vibration frequency, α is its starting phase, r is the vibration amplitude, $\mathbf{x}$ represents the (x, y) surface

Advances in Metrology for X-Ray and EUV Optics II, edited by Lahsen Assoufid, Peter Z. Takacs, Masaru Ohtsuka,
Proc. of SPIE Vol. 6704, 670402, (2007) · 0277-786X/07/$18 · doi: 10.1117/12.731421

position and $\Phi(\mathbf{x})$ is the interferometric starting phase (the phase to be recovered). For convenience, Eq. (1) is separated into a DC term and the signal of interest $s(\mathbf{x},t)$

$$s(\mathbf{x},t)=\frac{I_0V}{2}\left[\exp(i\Phi(\mathbf{x}))\exp(i\beta(t))+\exp(-i\Phi(\mathbf{x}))\exp(-i\beta(t))\right] \tag{2}$$

with $\beta(t)=2\pi\nu_0 t+r\cos(2\pi\nu_v t+\alpha)$ representing the actual phase shift variation experienced during the acquisition. Utilizing the Jacobi-Anger expansion,[14] Bessel functions properties[15] and integrating over the detector integration period τ, Eq. (2) becomes

$$\begin{aligned}
s(\mathbf{x},t)=&\frac{I_0V}{2}J_0(r)\mathrm{sinc}(\pi\nu_0\tau)\exp(i\Phi(\mathbf{x})+2\pi i\nu_0 t)+\\
&\frac{I_0V}{2}J_0(r)\mathrm{sinc}(\pi\nu_0\tau)\exp(-i\Phi(\mathbf{x})-2\pi i\nu_0 t)+\\
&\frac{I_0V}{2}\sum_{k=1}^{\infty}i^kJ_k(r)\mathrm{sinc}(\pi\tau(\nu_0+k\nu_v))\exp(i\Phi(\mathbf{x})+ik\alpha)\exp(i2\pi t(\nu_0+k\nu_v))+\\
&\frac{I_0V}{2}\sum_{k=1}^{\infty}i^kJ_k(r)\mathrm{sinc}(\pi\tau(\nu_0-k\nu_v))\exp(i\Phi(\mathbf{x})-ik\alpha)\exp(i2\pi t(\nu_0-k\nu_v))+\\
&\frac{I_0V}{2}\sum_{k=1}^{\infty}(-i)^kJ_k(r)\mathrm{sinc}(\pi\tau(-\nu_0+k\nu_v))\exp(-i\Phi(\mathbf{x})+ik\alpha)\exp(i2\pi t(-\nu_0+k\nu_v))+\\
&\frac{I_0V}{2}\sum_{k=1}^{\infty}(-i)^kJ_k(r)\mathrm{sinc}(\pi\tau(-\nu_0-k\nu_v))\exp(-i\Phi(\mathbf{x})-ik\alpha)\exp(i2\pi t(-\nu_0-k\nu_v))
\end{aligned} \tag{3}$$

Following standard PSI practice[16], the spectrum is first calculated with the Fourier transform:

$$S(\nu)=\int_{-\infty}^{\infty}s(t)\exp(-i2\pi\nu t)\,dt \tag{4}$$

producing

$$\begin{aligned}
S(\nu)=&\frac{I_0V}{2}J_0(r)\mathrm{sinc}(\pi\nu_0\tau)\exp(i\Phi(\mathbf{x}))\delta(\nu-\nu_0)+\\
&\frac{I_0V}{2}J_0(r)\mathrm{sinc}(\pi\nu_0\tau)\exp(-i\Phi(\mathbf{x}))\delta(\nu+\nu_0)+\\
&\frac{I_0V}{2}\sum_{k=1}^{\infty}i^kJ_k(r)\mathrm{sinc}(\pi\tau(\nu_0+k\nu_v))\exp(i\Phi(\mathbf{x})+ik\alpha)\delta(\nu-\nu_0-k\nu_v)+\\
&\frac{I_0V}{2}\sum_{k=1}^{\infty}i^kJ_k(r)\mathrm{sinc}(\pi\tau(\nu_0-k\nu_v))\exp(i\Phi(\mathbf{x})-ik\alpha)\delta(\nu-\nu_0+k\nu_v)+\\
&\frac{I_0V}{2}\sum_{k=1}^{\infty}(-i)^kJ_k(r)\mathrm{sinc}(\pi\tau(-\nu_0+k\nu_v))\exp(-i\Phi(\mathbf{x})+ik\alpha)\delta(\nu+\nu_0-k\nu_v)+\\
&\frac{I_0V}{2}\sum_{k=1}^{\infty}(-i)^kJ_k(r)\mathrm{sinc}(\pi\tau(-\nu_0-k\nu_v))\exp(-i\Phi(\mathbf{x})-ik\alpha)\delta(\nu+\nu_0+k\nu_v)
\end{aligned} \tag{5}$$

where $\delta(\nu)$ is the Dirac delta function. Time and frequency domain representations of the signal are distinguished by lower and upper case variables respectively. The surface phase profile is evaluated by calculating the spectral phase at the fundamental interference frequency ν_0 for each pixel in the field. The phase profile is thus

$$\hat{\Phi}(\mathbf{x}) = \arg(S(\mathbf{x},\nu_0) = \tan^{-1}\left\{\frac{\mathrm{Im}[S(\mathbf{x},\nu_0)]}{\mathrm{Re}[S(\mathbf{x},\nu_0)]}\right\}, \tag{6}$$

where the caret is used to indicate the measured interferometric phase rather than the true one. The terms in Eqs. (5) contribute to $\hat{\Phi}(\mathbf{x})$ only if the argument of the delta-function equals zero, which for the vibrationally induced spectral terms, occurs only when the vibration frequency satisfies $\nu_v = 2\nu_0 / k$. Combining the nonzero terms, the spectral component at ν_0 becomes

$$S(\mathbf{x},\nu_0) = \eta \exp(i\Phi(\mathbf{x})) + \bar{\mu} \exp(-i\Phi(\mathbf{x})), \tag{7}$$

where the bar over variables signifies the complex conjugate, with

$$\eta = \frac{I_0 V}{2} J_0(r)\,\mathrm{sinc}(\pi\tau\nu_0), \tag{8}$$

and

$$\bar{\mu} = \frac{I_0 V}{2} \sum_{k=1}^{\infty} (-i)^k J_k(r)\,\mathrm{sinc}(\pi\tau(k\nu_v - \nu_0)) \exp(ik\alpha)\delta(\nu_v - 2\nu_0/k). \tag{9}$$

Note that for small r, $J_0(r) \approx 1$ and $J_1(r) \approx r/2$, so as $\tau \to 0$, the first order term equals

$$S(\mathbf{x},\nu_0) = \frac{I_0 V}{2}\left(\exp(i\Phi(\mathbf{x})) - \frac{ir}{2}\exp(i(-\Phi(\mathbf{x}) + \alpha))\right) \tag{10}$$

which agrees with Huntley's result.[11]

Eq. (7) represents the interference spectrum computed by an infinitely sampled PSI algorithm in the presence of vibrations. The vibrational contribution is carried completely in the second term $\bar{\mu} \exp(-i\Phi(\mathbf{x}))$ and for a single pure vibrational tone μ has only one nonzero term, provided the vibration frequency satisfies $\nu_v = 2\nu_0 / k$. The analysis not only explains the 1st order sensitivity of PSI algorithms to vibrations at twice the phase-shifting frequency, but also provides insight into the higher order sensitivities, which occur at progressively smaller vibration frequencies. For large amplitude vibrations these higher order sensitivities can be a significant error contributor. This result is sufficiently important to verify, and Figure 1 displays the results of a simulation showing that the interferometric phase error has the greatest sensitivity at exactly those vibrational frequencies predicted by Eq. (7).

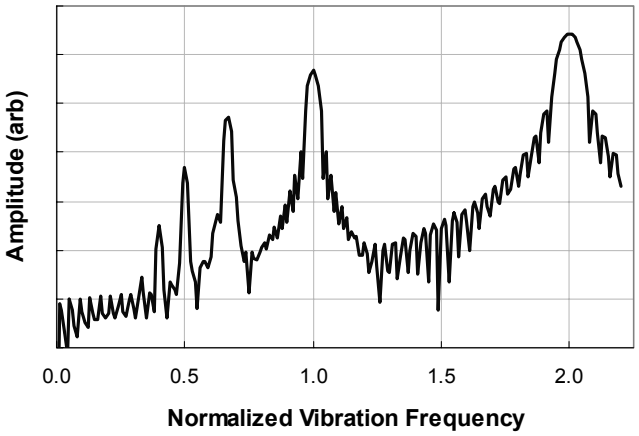

Figure 1: Phase error sensitivity of a PSI algorithm as a function of vibrational frequency normalized to the sample rate

Practical PSI algorithms are finite and only sparsely time-sample the interference, in which case the delta-functions must be replaced with the Fourier transform of the PSI sampling function. This substitution reduces spectral resolution and increases leakage, making the power from a single frequency leak across the measured spectrum. In practice therefore, many terms contribute to the sum in μ even if only a single vibrational tone is present, with the influence of the higher order terms increasing with vibration strength.

3. SUPPRESSING VIBRATION PHASE ERRORS

Since the surface profile is ultimately determined from the spectral phase, I can be write,

$$\exp(i\hat{\Phi}) = \frac{\eta \exp(i\Phi) + \overline{\mu} \exp(-i\Phi)}{\left|\eta \exp(i\Phi) + \overline{\mu} \exp(-i\Phi)\right|} \tag{11}$$

where the explicit dependence of Φ on $\mathbf{x}$ is omitted for clarity. Solving for $\exp(i\Phi)$ gives,

$$\exp(i\Phi) = \pm \exp(i\hat{\Phi}) \frac{\overline{\eta}}{|\eta|} \sqrt{\frac{1 - \overline{z} \exp(-2i\hat{\Phi})}{1 - z \exp(2i\hat{\Phi})}}\,, \tag{12}$$

where $z = \mu/\eta$. For an infinitely sampled intensity signal $\overline{\eta}/|\eta| = 1$, so the positive solution is taken since the measured phase must tend toward the true phase as the vibration amplitude tends to zero. For finite PSI algorithms, $\overline{\eta}/|\eta|$ may in general be complex depending on the PSI sampling coefficients c_j, with a value other than unity just representing a constant phase offset in the sampling sequence. Without loss of generality therefore, the value of $\overline{\eta}/|\eta|$ can be changed to unity by multiplying the algorithm sampling coefficients by an appropriate complex constant of unit magnitude without changing the algorithm dynamic response.

Equation (12) describes how to use the measured phase, which is corrupted by the vibrational disturbance, to recover the true phase. Unfortunately this relation is not practical since it depends on z, which itself depends on the vibration spectrum through μ. However, for vibrations with small enough amplitude, $|z| = |\mu/\eta| < 1$, and the radical can be expanded using the binomial theorem to obtain,

$$\exp(i\Phi) = \exp(i\hat{\Phi}) \sum_{n=0}^{\infty} \mathsf{g}_n \exp(-i2n\hat{\Phi}) \sum_{m=0}^{\infty} \mathsf{h}_m \exp(i2m\hat{\Phi}) \tag{13}$$

with coefficients $\mathsf{g}_n = \dfrac{\frac{1}{2}!}{(\frac{1}{2}-n)!n!}\left(-\overline{z}\right)^n$ and $\mathsf{h}_m = \dfrac{(-\frac{1}{2})!}{(-\frac{1}{2}-m)!m!}\left(-z\right)^m$. The product of the two sums produces a series of positive and negative odd harmonics of the measured phase

$$\exp(i\Phi) = \sum_{k=-\infty}^{\infty} g_k \exp(i(2k+1)\hat{\Phi})\,, \tag{14}$$

with the harmonic coefficients g_k given by

$$g_k = \begin{cases} \displaystyle\sum_{n=0}^{\infty} \mathsf{g}_n \mathsf{h}_{n+k} & k \geq 0 \\ \displaystyle\sum_{n=0}^{\infty} \mathsf{g}_{n-k} \mathsf{h}_n & k < 0 \end{cases}. \tag{15}$$

Close inspection of Eq. (15) provides the following excellent approximation for all vibration amplitudes of interest

$$g_k \cong -(2k-1)\overline{g}_{-k}\,, \tag{16}$$

from which Eq. (14) can be rewritten as

$$\exp(i\Phi) \cong \exp(i\hat{\Phi})\left(g_0 + \sum_{k=1}^{\infty}\left(g_k \exp(i2k\hat{\Phi}) - \frac{\bar{g}_k \exp(-i2k\hat{\Phi})}{2k-1} \right)\right). \tag{17}$$

Eq. (17) is a more practical representation of Eq. (12), since the harmonic coefficients can be evaluated from a measurement of the phase increments. It is important to note that this principle can be applied regardless of detector integration since the harmonic coefficients automatically account for the effect this has on the spectrum. Of course a practical limitation occurs if the vibration is severe enough to significantly degrade fringe contrast during the integration time, but in that case typically the PSI algorithm fails.

4. VC METHOD

The technique uses the spatial intensity variation between adjacent frames to calculate the phase increments between those frames; therefore illumination nonuniformity must first be measured and accounted for. Prior to the measurement, the light reflected from the reference surface alone provides a measure of the intensity distribution profile. This profile is used to correct each frame of interference data so that the measured interference is normalized everywhere to the same illumination intensity. A noteworthy feature of this method for background illumination measurement is its speed, accuracy and environmental insensitivity.

The phase increments between acquired frames are then evaluated by analyzing the change of the interference pattern using the initial surface profile derived from the chosen PSI algorithm. The phase increment calculation requires a full 2π of surface phase variation for optimum results so at least one fringe must be visible across the surface. Once the phase increments are determined, a variety of methods can be used to recalculate the profile, such as the least-squares method described in Ref. [10]. However, a least-squares analysis has increased broad-band noise characteristics due to its broad frequency acceptance, so we developed a proprietary method that calculates and subtracts only the vibration induced distortion from the PSI profile, thereby preserving the low noise character of the PSI calculated profile.

Figure 3 compares pre- and post-processed best-fit plane-removed profiles of a flat surface with about 5 fringes of departure measured with a well-known 13-frame PSI algorithm[17] in the presence of ~15nm amplitude vibrations. The vibrationally induced ripple is reduced by a factor of >25 while retaining the full spatial resolution. In particular the method does not introduce low spatial frequency form distortion, (which would occur if spatial filtering methods were employed to remove the ripple), or increased high frequency noise.

The technique can be applied to interferograms of any fringe complexity as long as at least one fringe is visible. Therefore the technique works with surfaces of any shape. Figure 3 compares pre- and post-processed best-fit sphere-removed profiles of a spherical surface with about 3 fringes of departure measured with the same PSI algorithm in the presence of ~25nm amplitude vibrations. The vibrationally induced ripple is again reduced by over a factor of 25.

As described, the technique only handles cavity motion along the optical axis (known as piston), but can be easily modified to account for test object rigid body motion if the image field is subdivided into quadrants and phase increments calculated in each quadrant independently. The quadrant phase increments can then be spatially fitted to account for piston, tip and tilt motion when calculating the final surface profile. Higher order vibrational motions can be accommodated with a greater number of image subdivisions. Note that each subdivision must have at least 2π of spatial phase variation for the local piston phase increment calculation. This Author has found that quadrant subdivision is adequate for the majority of applications.

Variation in the test surface reflectivity can also be accommodated if the spatial dependence of the reflectivity is measured; either directly using a technique similar to that for measuring intensity uniformity, or by inferring the reflectivity through a measure of the interference contrast.

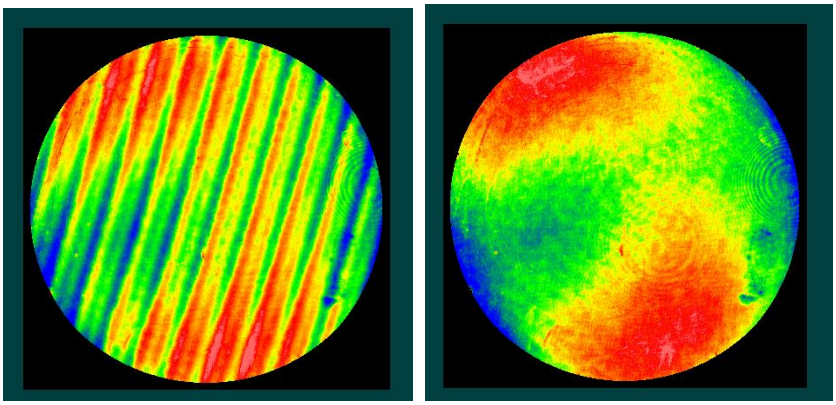

Figure 2: Measurement of a flat part with ~5 fringes of tilt disturbed with a 15nm amplitude vibration at a frequency of ¼ of the frame rate before (left) and after (right) processing with the VC algorithm. The 15nm PV ripple observed in the original profile was reduced by >25X.

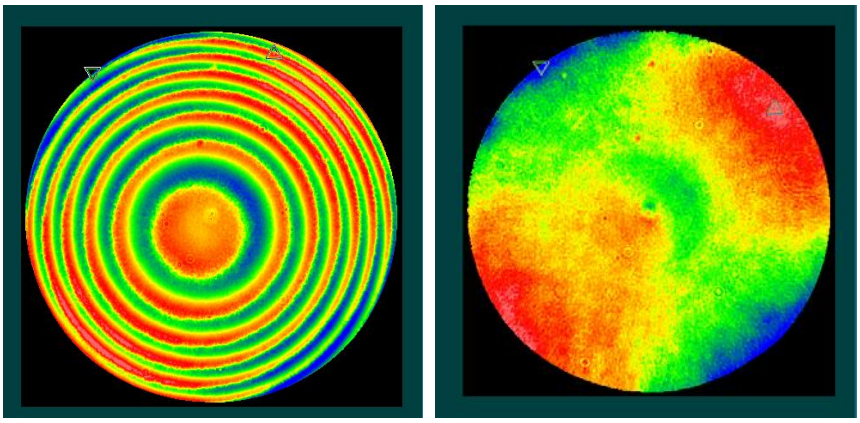

Figure 3: Measurement of a spherical part with ~3 fringes of departure disturbed with a 25nm amplitude vibration at a frequency of ¼ of the frame rate before (left) and after (right) processing with the VC algorithm. The 20nm PV ripple observed in the original profile was reduced by >25X.

5. PERFORMANCE CHARACTERISTICS

The method's performance was analyzed as a function of vibration frequency and amplitude using phase error sensitivity spectra (Figure 4) out to third order in the harmonic coefficients. The phase error sensitivity spectrum is simply the predicted rms surface distortion normalized to the vibrational amplitude as a function of vibrational frequency normalized to the camera frame rate. The predictions indicate that the method works best for small amplitude vibrations, where the sensitivity to external vibrations is reduced by several orders of magnitude across the vibrational spectrum. As the amplitude increases, the sensitivity of the VC technique to vibrations increases, but still provides improvement over the PSI algorithm alone for all vibration frequencies. Beyond 60nm vibration amplitudes the PSI algorithm itself fails and therefore a correction cannot be determined.

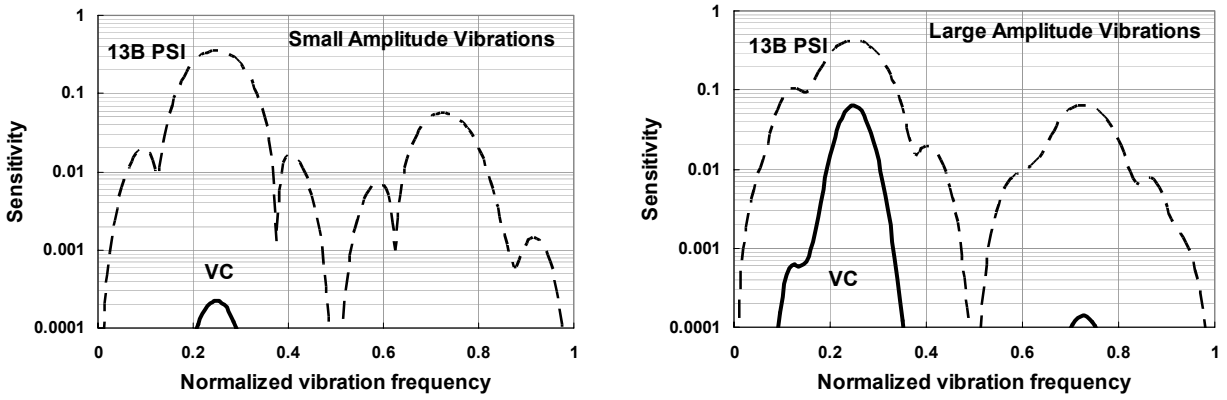

Figure 4: Phase error sensitivity for the 13-frame algorithm (dashed line) and VC (solid line) for small amplitude (5nm) and large amplitude (50nm) vibrations.

6. SUMMARY

I described an analytic correction technique for suppressing vibrationally induced distortion in phase-shifting interferometry. The technique reduces surface distortion by 100X for small amplitude vibrations and >8X for large amplitude vibrations. The technique can be applied to any PSI algorithm or surface shape and retains full sampling resolution.

REFERENCES

[1] J. Greivenkamp and J. Bruning, "Phase Shifting Interferometry", Chap. 14, of "Optical Shop Testing", 2nd Ed., J. Wiley pub, edited by D. Malacara.
[2] P. de Groot, "Vibration in phase shifting interferometry," J. Opt. Soc. Am. A, 12(2), 354-365 (1995)
[3] P. Winzinowich, "Phase shifting interferometry in the presence of vibration: a new algorithm and system," Appl. Opt. **29,** 3271–3279 (1990).
[4] L. Deck, "Vibration-resistant phase-shifting interferometry," Appl. Opt. 35, 6655-6662 (1996)
[5] L. Deck and P. de Groot, "Punctuated quadrature phase-shifting interferometry," Opt. Lett. 23 (1) 19-21 (1998)
[6] M. Takeda, H. Ina, and S. Kobayashi, "Fourier-transform method of fringe pattern analysis for computer based topography and interferometry," J. Opt. Soc. Am. 72, 156-160 (1982)
[7] B. Kimbrough, J. Millerd, J. Wyant, J. Hayes, Proc. SPIE 6292 (2006)
[8] M, Kujawinska and D. Robinson. "Multichannel phase-stepped holographic interferometry," Appl. Opt. 27(2), 312-320
[9] G. S. Han and S. W. Kim, "Numerical correction of reference phases in phase-shifting interferometry by iterative least-squares fitting," Appl. Opt. 33, 7321-7325 (1994)
[10] J. Greivenkamp, "Generalized data reduction for heterodyne interferometry," Opt. Eng., 23, 350 (1984)
[11] J. M. Huntley, "Suppression of phase errors from vibration in phase-shifting interferometry," J. Opt. Soc. Am. A, 15(8), 2233-2241 (1998)
[12] L. Deck, "Environmentally Friendly Interferometry," Proc. SPIE, 5532, 159-169 (2004)
[13] The techniques described in this paper are protected by U.S. and foreign patents or patents pending.
[14] $\exp[iu\cos(\alpha)] = J_0(u) + 2\sum_{k=1}^{\infty} i^k J_k(u)\cos(k\alpha)$
[15] $J_k(-r) = \begin{cases} -J_k(r) \ \ for\ k\ odd \\ J_k(r) \ \ for\ k\ even \end{cases}$
[16] K. Freischlad and C. L. Koliopoulos "Fourier description of digital phase-measuring interferometry," J. Opt. Soc. Am. A7, 542-551 (1990)
[17] P. de Groot, "Derivation of algorithms for phase-shifting interferometry using the concept of a data-sampling window," Appl. Opt. 34(22), 4723-4730 (1995)